Applied Catalysis B: Environmental 200 (2017) 420–427

Contents lists available at ScienceDirect

Applied Catalysis B: Environmental

journal homepage: www.elsevier.com/locate/apcatb

Structuring $Pt/CeO_2/Al_2O_3$ WGS catalyst: Introduction of buffer layer

M. González-Castaño*, S. Ivanova, O.H. Laguna, L.M. Martínez T., M.A. Centeno, J.A. Odriozola

Departamento de Química Inorgánica e Instituto de Ciencia de Materiales de Sevilla (ICMS), Centro mixto CSIC-Universidad de Sevilla, Avda. Américo Vespucio 49, 41092 Sevilla, Spain

ARTICLE INFO

Article history:
Received 30 May 2016
Received in revised form 13 July 2016
Accepted 19 July 2016
Available online 20 July 2016

Keywords:
WGS
Monoliths
Buffer layer
Platinum catalysts
Structured catalyst

ABSTRACT

This work is devoted to the development of novel structured catalytic system for WGS reaction. The new concept is related to the presence of a pre-catalytic "buffer" layer formed by WGS-inert oxide, i.e. not involved in CO conversion, but able to increase the number of participating sites in water dissociation step during the reaction. The performance of the proposed systems appears to depend strongly on the stream composition, being its effect beneficial in highly reducing atmospheres making it ideal for clean-up application. An increment of the partial kinetic order for water species is observed and reveals the key role of the water activation for superior catalytic behavior.

© 2016 Elsevier B.V. All rights reserved.

1. Introduction

The new challenge, leading to the renovated interest on the water-gas-shift (WGS) process, concerns the development of catalysts able to implement the hydrogen technology (hydrogen production and purification) on portable applications. The WGS reaction is characterized by the high contact times needed to achieve high CO conversions being also moderately exothermic. These facts imply high reactor volume making difficult its implementation in actual on-board H_2 production and application processes [1]. Catalytic Wall Reactors appear to be an alternative for reducing the catalyst bed volume while maintaining high catalytic efficiency. In this line, longitudinal parallel channel monoliths or micromonoliths are an interesting solution by itself and may also provide clues on the behavior of microreactors [2–4]. Fu et al. [5] studied WGS catalysts structured on metallic monoliths. They claim that monolith-based designs provide the necessary mechanical strength and allow a better platinum use and, hence, lower the reactor volumes. Indeed, it has been reported that micromonolithic reactors can diminish the WGS reactor units volume by a factor of two [6]. Farrauto et al. [1,7] also reported promising results regarding activity and stability for Pt based catalysts through combining metallic micromonolithic devices and proper catalyst designs.

Therefore, these structured systems are a valuable alternative to packed fixed bed reactors (PBR) allowing higher space velocities and lower pressure drops. The process intensification is normally related to the higher surface to volume ratio provided by micromonoliths resulting in volume reduction that allows higher efficiencies. The micromonolith structures may be ceramic or metallic.

The metallic ones present high thermal conductivities, lower heat capacities and superior thermal and mechanical shock resistances [8,9]. Moreover, among the metallic substrates, the aluminum-alloyed ferritic stainless steel (FeCrAl®) monolithic structures accomplish show an excellent stability in high carbon activity atmospheres reducing corrosion phenomena due to carburization [10–13]. Particularly, the improved mass and heat transferences allowed by the use of structured catalysts are of mandatory importance for the WGS reaction [14,15]. Indeed, considering that the WGS is exothermic and thermodynamically limited, optimal temperature control, as that provided by metallic micromonoliths, becomes a very interesting feature which should enhance the catalytic performance and avoid or minimize the hot spot formation.

These effects must be considered in practical situations; otherwise, wrong predictions with respect to the catalytic behaviors may result. Considering that those processes are controlled by the layer thickness, the use of micromonolithic structures should improve the diffusional processes and allow a better control of the reaction through an appropriate catalytic layer thickness providing a bet-

* Corresponding author.
E-mail address: miriam.gonzalez@icmse.csic.es (M. González-Castaño).

http://dx.doi.org/10.1016/j.apcatb.2016.07.039
0926-3373/© 2016 Elsevier B.V. All rights reserved.

Fig. 1. Structured catalysts design.

ter temperature control hindering the hot spot formation [16,17]. Therefore, the layer thickness should be well-controlled in order to maintain the enhancement of the transport phenomena provided by the micromonoliths.

Several mechanisms have been proposed in the literature for WGS reaction, these include as intermediates carboxyl, carboxyl hydroxyl, redox, dual hydroxyl or one step carboxyl formation. However, whatever the mechanism most authors propose the water activation step as the rate limiting one for the WGS reaction on a wide selection of metallic active phases including Co, Cu, Ni, Ag, Rh, Ir, Au and Pt [18–22]. More precisely, Phatak et al. [22] proposed the hydroxyl dissociation as rate-limiting step for Pt and other noble metals on comparing the binding energies of H_2O, OH and H species on metals. In accordance, the superior WGS rate exhibited by Pt metal was also related directly to the slightly lower water dissociation barrier. Actually, the water activation step is commonly associated to the support oxygen vacancies becoming then, a key chemical site for the WGS reaction [23]. Therefore, oxygen vacancies play an important role concerning water molecules dissociation that will occur on the support [14,24].

Likewise the majority of the noble metals, the Pt catalysts exhibit significant improvement when combined with reducible oxides such as CeO_2. This boosting effect is normally related to the existence of Ce^{4+}/Ce^{3+} redox pair and, more precisely, to the key role of the oxygen vacancies as active sites for the water dissociation step [25].

In this study different amounts of Pt(2%)/CeAl catalyst were washcoated on micromonoliths. The catalyst layer deposition was carefully controlled for obtaining a series of catalytic wall reactors (CWR) having different catalyst thicknesses. Besides this, a series of CWRs constituted by two different layers were prepared: (i) a first layer based on CeO_2-Al_2O_3, named *buffer* layer and (ii) a Pt(2%)/CeO_2-Al_2O_3 layer, the catalyst layer, supported over the buffer one. For such system, equal amounts were deposited for each catalytic layer supported. This procedure was chosen based on the concept that increasing the concentration of cerium oxide in the system should increase the number of oxygen vacancies and therefore the number of water activation sites. The idea was to introduce a second active sublayer able of increasing the water dissociation capacity and buffer the amount of water species in the WGS reaction. If this hypothesis is correct, the incorporation of the buffer layer should increase the catalytic performance. The designed systems were tested in two WGS mixtures, being the difference between them the presence of CO_2 and H_2. The later could proportionate more information regarding the effect caused by the buffer presence as a function of changes in the character of the WGS mixture from more to less reductive one.

2. Experimental

2.1. Catalyst synthesis

A commercial 20 wt.% CeO_2–80 wt.% Al_2O_3 solid (Puralox, Sasol) was used as catalyst support and buffer. Platinum (2 wt.% nominal value) was deposited by wet impregnation using tetrammineplatinum(II) nitrate solution (Johnson Matthey) as precursor. The resulting solid was calcined at 350 °C for 8 h at 5 °C/min heating rate. For the sake of briefness, support and catalyst, CeO_2/Al_2O_3 and Pt(2%)/CeO_2/Al_2O_3 are labelled CeAl and Pt/CeAl, respectively.

2.2. Preparation of metallic micromonolith substrate

The cylindrical micromonolithic structures were manufactured by rolling up, around a spindle, flat and corrugated foils of 50 μm thick Al-alloyed ferritic stainless steel (Fecralloy®) by a procedure largely described [26,27]. These 3 cm height and 1.6 cm in diameter micromonolithic structures have a geometric surface area of 540 cm^2 and a cell density of 2067 cells per square inch (cpsi). Prior the catalyst deposition procedure the micromonoliths were thermally treated at 900 °C for 22 h in order to grow a α-Al_2O_3 surface layer, which will improve the subsequent catalyst adhesion [28].

A washcoating procedure was selected for depositing all catalytic layers. In this method, stable non-settling slurries are prepared for every synthesized solid. [29,30] A careful study of the rheological properties of the suspensions resulted in a formulation that optimizes surface tension and viscosity of the slurry. The optimum composition appeared to be 1.96 wt.% of polyvinylalcohol (PVA) solution (1.5 wt.% PVA in water), 17.65 wt.% of colloidal Al_2O_3 suspension (Nyacol, 20 wt.% in water), 18.14 wt.% of catalyst and 62.25 wt.% of water. Prior to their use the solids were grinded and sieved to particle sizes around 10 μm in order to increase suspension stability. The rheological properties of the suspension were controlled by the additives; colloidal alumina and PVA were added in order to increase the suspension stability and to help rising the

suspension within the monolith channels. The prepared suspension allows the deposition of around 80 mg of solid at each coating step. As previously reported the metal substrate may influence the activity and selectivity of the washcoated catalyst [31–34]. In order to highlight this possible influence the slurries were dried and further calcined as previously described for the monolithic catalysts. The slurries prepared this way are named S-Pt/CeAl and S-CeAl for the calcined suspension of the Pt/CeAl catalyst and the CeAl support, respectively.

Three different micromonoliths loaded nominally with 0.3, 0.6 and 0.8 g of the Pt/CeAl catalyst were prepared and named M0.3, M0.6 and M1, respectively.

The effect of the buffer layer was studied over structured devices containing 0.3 g of the Pt/CeAl catalyst deposited onto a 0.4 g CeAl buffer-coated micromonolith. This structured bilayer catalyst was named M0.3-B0.3. A scheme of the structure of the micromonolith together with the actual amounts of buffer and catalyst deposited on the wall of channels is presented in Fig. 1.

2.3. Characterization techniques and catalytic activity

The chemical composition of the prepared catalysts was determined by X-Ray microfluorescence spectrometry (XRMF) employing an EDAX Eagle III spectrophotometer which rhodium radiation source.

The textural properties were analyzed by N_2 adsorption-desorption experiments at liquid nitrogen temperature. The measurements were performed on a Micromeritics Tristar 22 instrument. Before the analysis, the samples were degassed for 2 h at 150 °C in vacuum. For the textural properties of the monoliths, a homemade, especially designed, sample holder was used allowing the analysis of the whole monolith.

The X-ray Ray Diffraction (XRD) patterns were recorded on a X'Pert Pro PANalytical instrument employing Cu Kα radiation (45 KV, 40 mA) over 10–95° 2θ range with 0.05° step size and 240 s step time.

Scanning electron microscopy (SEM) analysis was performed on a JEOL 5400 microscope equipped with an EDS analyzer (Oxford Link). The adherence between catalyst/buffer layer and substrate was analyzed immersing the micromonolith in acetone for 30 min in an ultrasonic bath. The adherence was estimated as the difference in weight with respect to the untreated sample.

The catalytic activity was measured in a tubular flow reactor at atmospheric pressure in the 180–350 °C temperature range using either a 4.5% CO, 30% H_2O and 66.5% N_2 WGS flow, named model conditions, or a reformate out-gas feed stream containing 7% CO, 9% CO_2, 50% H_2 and 30% H_2O (balanced with N_2), this composition simulates the outlet of a typical ethanol reformer reactor, named real conditions. This later composition allows the variation of the partial pressures of each component maintaining constant the total flow (400 ml min^{-1}). Prior to its use the catalysts were pretreated at 350 °C for 2 h in H_2 (10 vol.% in N_2). Carbon oxides compositions were analyzed using an ABB gas analyzer and the activity is presented as percentage of CO conversion.

For the powder samples, 1 g of sample (bed volume = 1.5 cm^3) and a total gas stream of 100 mL/min were employed. All the powder samples were sieved and the 600–800 μm fractions retained. The tests were performed at GHSV = 4000 h^{-1} and WHSV = 6 L g^{-1} h^{-1}. For the structured catalysts, two different GHSV (4000 and 2000 h^{-1}) were employed with their corresponding WHSV (L g^{-1} h^{-1}). The GHSV (h^{-1}) was defined as the ratio of total gas flow (cm^3 h^{-1}) and the catalyst bed volume (cm^3) meanwhile the WHSV (L g^{-1} h^{-1}) represents the normalization of the total gas flow L h^{-1} by the weight of the catalyst and/or active phase (g^{-1}).

Table 1
Chemical composition and specific surface of the prepared solids.

	Al_2O_3 (wt.%)	CeO_2 (wt.%)	Pt (wt.%)	S_{BET} (m^2/g)
Pt(2%)/CeAl	77.6	20.2	2.2	142
CeAl	79.0	21.0	–	146
S-Pt(2%)/CeAl	80.7	17.3	2.0	156
S-CeAl	82.8	17.2	–	187

Table 2
Specific surface, layer thickness (LT) and particle sizes estimated for the prepared structured solids.

	S_{BET} (m^2/g)	LT (μm)	r (μm)
M0.3	152	3.5	10.5
M0.6	183	6.6	19.8
M1	190	8.7	26.1
M0.3-B0.3	143	8.6	26.8

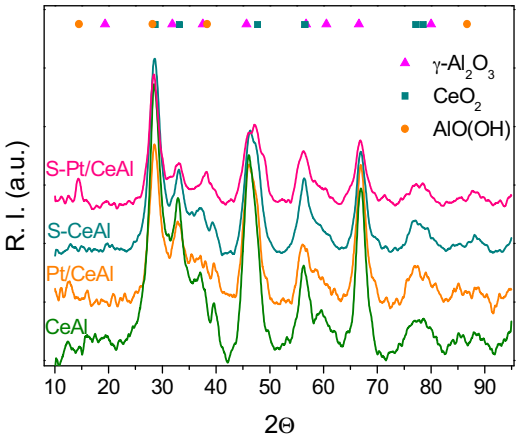

Fig. 2. XRD of the prepared powder catalysts.

3. Results and discussion

The chemical composition of the synthesized samples is shown in Table 1. The actual platinum content was very close to the nominal one (2 wt.%). Colloidal alumina addition to the slurry formulation accounts for the differences in the alumina content of the slurry and the prepared powders.

The textural properties of the prepared catalysts are also shown in Table 1. The calcined suspensions exhibit similar surface areas and pore diameter (D_{pore}) values than their parent powders, being the differences related to the amount of colloidal alumina. After structuring the catalysts the textural properties of the catalytic layers hardly changes, Table 2.

From the XRD diffraction analysis, only cubic CeO_2 fluorite and γ-Al_2O_3 are detected in all samples, Fig. 2. It is worth to mention that no important changes occur during the washcoating process being the suspension very similar to the initial solid. Nevertheless in the case of the S-Pt/CeAl catalyst, diffractions attributed to the boehmite phase, γ-AlO(OH) (JCPDS 21-1307) originated from the colloidal alumina are also observed. However, for the S-CeAl suspension, these diffractions are not detected. On the other hand, no platinum diffractions can be discerned, due either the low platinum content and/or to platinum particles sizes lower than the detection limit (<4 nm). The platinum dispersion estimate by CO adsorption resulted to be ~58%, as reported elsewhere [25].

The homogeneity of the washcoated layer was studied by SEM. A microphotograph obtained for the M1 sample is shown in Fig. 3 as an example. A well-dispersed catalyst layer is observed (Fig. 3a). The EDX analysis (Fig. 3b), in transversal section, shows firstly a

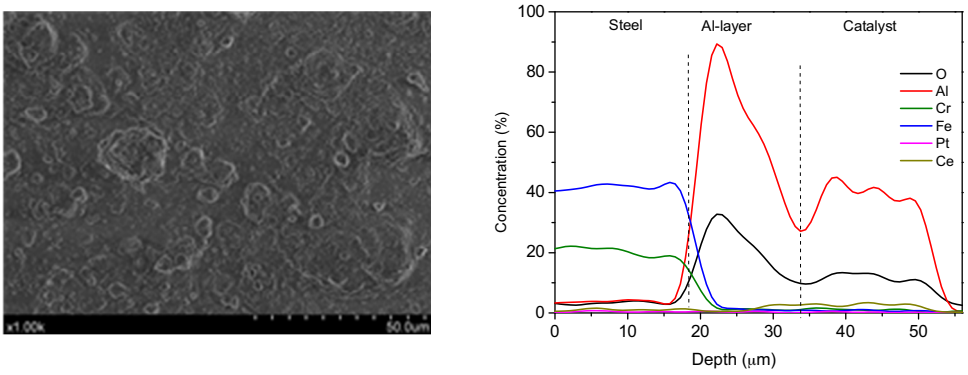

Fig. 3. SEM microscopy: (a) front microphotograph; (b) mapping elemental analysis.

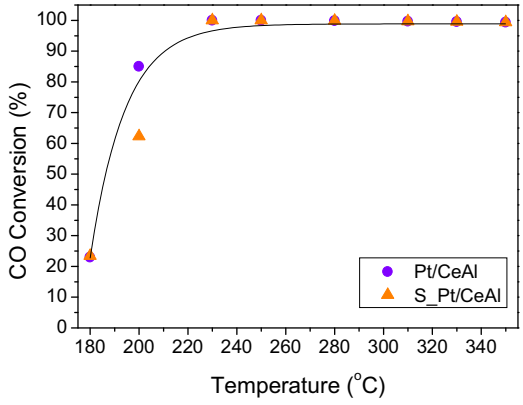

Fig. 4. Catalytic activity in "model" conditions of all powder samples. GHSV = 4000 h^{-1}, WHSV = 6 L h^{-1} g^{-1}.

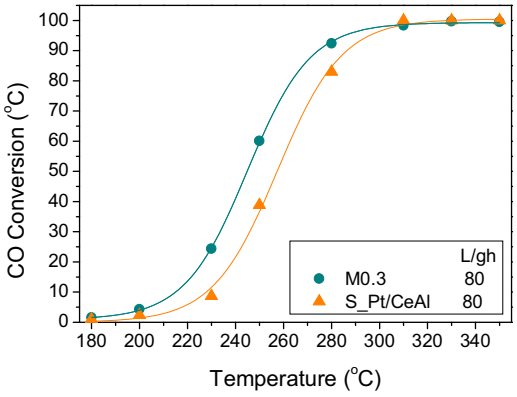

Fig. 5. Catalytic activity in "model" conditions of powder S-Pt/CeAl and M03 structured catalyst, tested at equal L/gh and GHSV = 4000 h^{-1}.

region rich in Fe and Cr corresponding to the stainless steel substrate followed by a zone composed by alumina grown during the oxidizing pretreatment of the substrate and then, the catalyst layer mainly composed by Al, Ce and O. No Pt was detected due to the lower quantity of the later in comparison to all the other elements. The adherence test resulted in 97 wt.% of the catalyst preserved on the substrate surface after the test indicating that the powders were well fixed on the metallic structures.

Table 2 presents an estimate of the catalyst layer thickness (LT) for all structured catalysts. For that purpose, the geometrical area of the micromonolith (540 cm^2), the actual amount and the chemical composition of all deposited solid are considered to calculate the compact volume using theoretical density values. The total volume was estimated by adding the calculated compact volume to the pore volumes of the calcined slurries. For the sake of comparison with packed bed reactors, the layer thickness is transformed in the equivalent radius of spherical particles. The calculated equivalent particle sizes for these catalytic layer thicknesses are also presented in Table 2.

The catalytic behavior of the powder samples was firstly tested in order to determine any change induced during the preparation of the slurry, Fig. 4. As could be observed the catalytic activity of the Pt/CeAl hardly changes after the formulation of the suspension.

As expected, structuring of the catalyst results in higher efficiencies on the WGS reaction, Fig. 5. In this figure, the catalytic activity of the M0.3 monolith and 0.3 g of the S-Pt/CeAl slurry are compared. The so call model mixture was used for the catalytic test run at 80 L g^{-1} h^{-1}. Both, improved mass and heat transport may account for this behavior. This result is in agreement with the study of Fu et al. [5] that observed improved catalytic performances for lower Pt loadings upon structuring the WGS catalysts. Farrauto et al. [1,7] also reported promising activity and stability results through combining metallic micromonolith devices with Pt based catalysts.

The effect of the catalyst loading (layer thickness efficiency) was also studied in order to determine if the gradual increase of the layer thickness resulted in higher catalytic activities or, on the contrary, mass and heat transfer capacities hinder the effect provided by the highest number of active sites. In order to evaluate the effect that the internal mass transfer have on the catalytic behavior, the effectiveness factor (η) was calculated for the M0.3, M0.6 and M1 monoliths. The effectiveness factor, η, is estimated through the calculation of the dimensionless diffusion parameter, ϕ, the sensitivity of the reaction rate to temperature, γ, and the maximum temperature variation which could exist within the particle relative to the boundary temperature, β. The Weisz and Hicks methodology [35] is adopted and the following expressions are employed.

$$\frac{dn}{dt} = k_o C_o y \exp\left\{\gamma\beta(1-y)/\left[1+\beta(1-y)\right]\right\} \quad (1)$$

$$\text{being } y = \frac{c}{c_0},\ \beta = \frac{C_o H D}{k T_o} = \left(\frac{\Delta T}{T_o}\right)_{\max} \text{ and } \gamma = \frac{Q}{R T_o}$$

where $\frac{dn}{dt}$ represents the rate of reaction, C_o is the CO (limiting reactive) concentration, H the enthalpy of the WGS reaction, k thermal conductivity of the catalyst, D the effective diffusivity calculated for the catalyst according to the expression proposed by Potemkin et al. [36] considering the molecular and Knudsen diffusions. If we reformulate the expression 1 assuming spherical particles, Eq. (2) gives directly the relation between the effectiveness factor η,

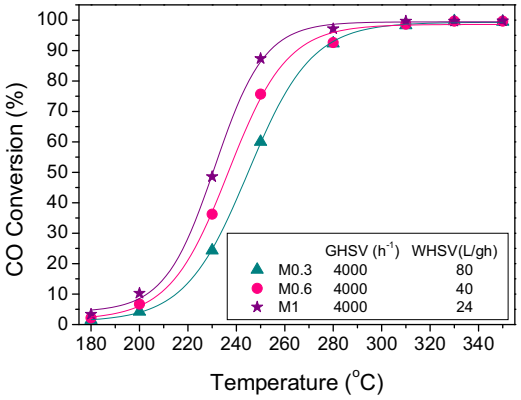

Fig. 6. Catalytic activity in "model" conditions of M0.3, M0.6 and M1 samples, at equal GHSV = 4000 h^{-1}.

the diffusion parameter, ϕ, the sensitivity of the reaction rate to temperature, γ, and the maximum temperature variation, β.

$$\frac{d^2y}{dx^2} + \frac{2dy}{xdx} = \Phi_0^2 y exp\left\{\gamma\beta(1-y)/\left[1+\beta(1-y)\right]\right\} \quad (2)$$

where $\Phi_0 = R\sqrt{(k_0/D}$ At boundary conditions y(1) = 1 and $\left(\frac{dy}{dx}\right)_{x=0} = 0$ and x = r/R the effectiveness factor η adopts numerical value and represents the ratio of the actual reaction rate to that which will be produced by the catalyst particle if no gradients of temperature and concentration are detected.

On the other hand, the efficiency factor estimate also requires a kinetic equation. Although a kinetic law was not developed for our catalyst, being this most convenient, literature data on WGS kinetic studies may provide, as it will see below, a rate law accurate enough for these estimates. The WGS kinetic has been widely reported in literature for several systems [15,36–40]. Among them, Germani et al. [40] reported a kinetic study properly obtained for a very similar system based in $Pt/CeO_2/Al_2O_3$. The kinetic law stated on this study is presented in Eq. (1).

$$-r_{CO}\left(\frac{molCO}{s\cdot kg_{cat}}\right) = \left(1.3\cdot 10^6\right)\times\left(e^{-\frac{86000}{RT}}\right) \times CO^{0.13}\times H_2O^{0.49}\times H_2^{-0.45}\times CO_2^{-0.12} \times\left(1-\frac{H_2\times CO_2}{K_{eq}\times CO\times H_2O}\right) \quad (3)$$

$$K_{eq} = e^{\left(\frac{4577.8}{T}-4.33\right)} \quad (4)$$

where . states for the apparent reaction rate expressed in moles converted CO per second and kg of catalyst, CO, H_2O, H_2, CO_2 are set for the gas inlet concentrations and K_{eq} refers to the equilibrium WGS constant at a given temperature.

No matter the value, that adopts the β parameter, lower ϕ values are obtained for our systems and temperatures, which lead to efficiency factors above 1 indicating the absence of diffusional intraparticle control. Therefore, it can be stated that diffusional processes does not influence the WGS activity of the structured catalysts, this allowing superior catalytic performances on increasing the amount of catalyst deposited on the micromonolithic structures at least for the thickness variation tested in this study, Fig. 6. Thus, the benefits provided by the process intensification are not limited by the catalytic layer thickness, which is in good agreement to data previously reported. For instance, Laguna et al. [17] recently demonstrated the absence of significant diffusional limitations controlling the catalytic performances for layer thicknesses around 10 μm. Moreover, Potemkin et al. [36] established a limit slightly higher for the layer thickness, above 20 μm, for which the diffusional processes does not control the reaction rate. Also in concordance, Farrauto et al. [1] reported that WGS structured catalysts are usually not pore diffusion limited. Therefore, the effect of the presence of a buffer layer should be also properly evaluated implying that behavior differences can be mainly related to chemical features.

By running the WGS reaction in model conditions (4.5 % CO + 30 % H_2O + N_2 balance) on different micromonoliths the absence of pore diffusion limitations was also checked, Fig. 7. Experimental limitations related to the operating range of the mass flow controllers prevent the comparison of all three micromonoliths at the same WHSV. Therefore, only the M0.3 and M0.6 micromonoliths were compared at 40 $L\,g^{-1}\,h^{-1}$ whereas the M0.6 and M1 ones were compared at *ca.* 20 $L\,g^{-1}\,h^{-1}$. Fig. 7 represents the catalytic activity of these micromonoliths. It is clear from the figure that on increasing the catalyst loading the catalytic activity proportionally increases while keeping constant the WHSV. Therefore, as it should be expected from the calculations of the effectiveness factor, pore diffusion limitations can be excluded in the studied monoliths.

The addition of a buffer layer behind the catalytic one, on the studied monoliths, should not affect the mass transport properties since the thickness of the catalytic layer remains constant. However, heat transport properties might be affected since the ceramic layer thickness is increased by the presence of the buffer. The monoliths containing a buffer layer have been tested in model conditions at both 2000 h^{-1} and 4000 h^{-1}. Fig. 7 presents the CO conversion as a function of temperature; it is clear that the buffer layer hardly influences the catalytic activity at least in these ideal conditions.

This effect was controlled by the comparison of the M0.3 and M0.3-B0.3 micromonoliths in model conditions at GHSV of 4000 h^{-1}. Fig. 8 presents the obtained CO conversion as a function

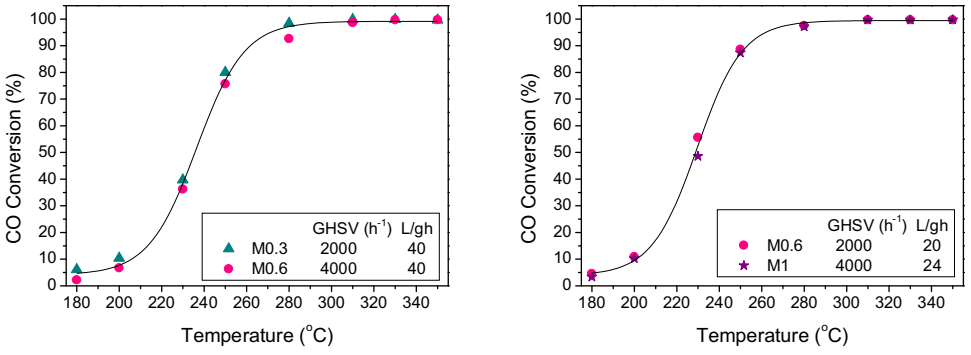

Fig. 7. Catalytic activity in "model" conditions, catalyst loading effect.

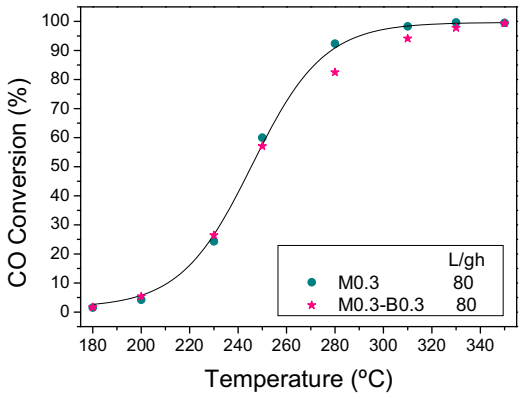

Fig. 8. Catalytic activity in "model" conditions, buffer presence effect, at 4000 h^{-1}.

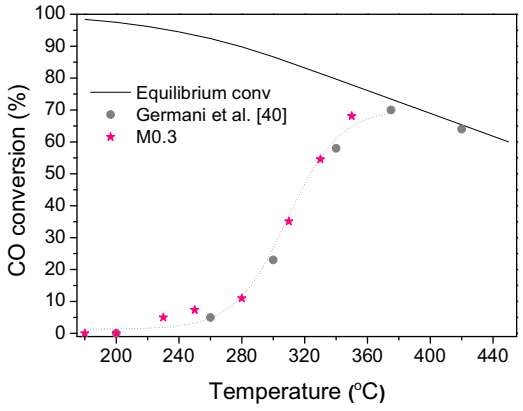

Fig. 9. Comparison of the M0.3 monolith operated at WHSV = 80 L g^{-1} h^{-1} under a reactive flow of 50% H_2, 7% CO, 9% CO_2, 30% H_2O, balance N_2 and data from Germani et al. [40] for a two platelet microreactor operated at WHSV = 73 L g^{-1} h^{-1} under a reactive flow of 32.2% H_2, 9,6% CO, 8.4% CO_2, 23% H_2O, balance Ar.

of temperature and it is clear that the buffer layer hardly influences the catalytic activity, which confirms that any changes will result only from the chemical nature of the buffer.

Testing the bilayer catalyst in a simulated out-gas feed stream containing 7% CO, 9% CO_2, 50% H_2 and 30% H_2O (balanced with N_2) the CO equilibrium conversion decreases and shift to higher temperatures, Fig. 9. In this figure the CO conversion is compared to that obtained by Germani et al. [40] for a two platelet microreactor coated with 1.4%$Pt/CeO_2/Al_2O_3$ catalyst operated at ~73 L g^{-1} h^{-1} and a reactive flow with a similar composition to that used in the present work (32.2% H_2, 9.6% CO, 8.4% CO_2, 23% H_2O, balance Ar). Despite the small differences in Pt loading, WSHV and reactive flow composition the catalytic activity in both the monolith and the microreactor device is similar. Therefore, it can be assumed, as for the effectiveness factor calculation, that the same rate law may fit our experimental results but just considering the different platinum loading and dispersion for the pre-exponential value of the Arrhenius expression, Eq. (1).

However, the presence of the buffer clearly outperforms the catalytic activity if the monoliths are tested in a simulated out-gas reactive flow, Fig. 10a. In these conditions, the presence of the buffer layer roughly duplicates the turnover frequency at 260 °C (5.6 for M0.3-B0.3 vs. 3.86 $mmol_{CO}$ s^{-1} kg_{cat}^{-1} for M0.3). The catalytic activity enhancement must be ascribed to the presence of the buffer layer since neither the loading nor the nature of the active sites has changed in $Pt/CeO_2/Al_2O_3$ catalyst. Moreover, the presence of the buffer layer does not affect the activity of the $Pt/CeO_2/Al_2O_3$ catalyst in the so-called model conditions, Fig. 8. The difference must be ascribed to a modification of the CeO_2/Al_2O_3 buffer layer in the presence of the outlet reformer surrogate.

A comparison of the observed and calculated reaction rates for the monoliths, assuming the rate law proposed by Germani et al. [40], is shown in Fig. 10b. There is an excellent agreement between the observed and calculated reaction rates for the M0.3 catalyst with all data fitting a straight line with a slope of 1.00 ± 0.05. However, when testing the monoliths that contain the buffer layer (M0.3-B0.3) the slope of the straight line is much higher (1.42 ± 0.08) accounting for the observed increase in the catalytic activity (Fig. 10b). The presence of the buffer layer does not affect the catalyst nature and therefore, the intrinsic activity should not be affected by its presence; hence the Arrhenius plot parameters must remain unchanged, as they must present the same CO adsorption enthalpy and coverage.

In order to understand the obtained results, Table 3 presents a summary of reported reaction orders and activation energies for Pt/Al_2O_3 and Pt/CeO_2 catalysts. The main differences in reaction orders are observed when carbon dioxide and hydrogen are not included in the calculation of the rate law [41,42]. In general, on including the CO_2 and H_2 effect on the WGS reaction rate, the apparent reaction orders and activation energy values are quite close despite the differences in the support nature, Pt loading and feed stream composition. The major difference between all of these studies occurs for the apparent reaction order for water that varies in the 0.44–1.10 range. Obviously, these differences must be associated to the presence of rhenium and/or the different nature of the support.

The apparent reaction order for carbon oxide is close to zero for all catalysts referenced as stated by Phatak et al. [42]. The weak interaction of CO_2 with the Pt surface is responsible for its negative, close to zero, reaction order. The decrease in the binding strength of CO adsorbed on Pt as the coverage increase [43–46] may account for the observed variation in the reaction order for CO, varying in the [−0.05, +0.14] range (Table 3), together with the negative order for H_2. As far as the CO surface coverage increases, its binding energy to the Pt surface decreases and hence, the H_2 inhibition of the WGS activity increases [47].

Phatak et al. [42] suggest that the negative and close to −0.5 apparent reaction order for H_2 implies that after CO attains its saturation coverage, atomic hydrogen will be the dominant surface species on the remaining Pt sites. The increase in the surface coverage of atomic hydrogen results in fewer sites available for water activation of the Pt surface, which results in the inhibition of the WGS reaction. In their explanation for the different rate laws observed they argued that the calculated range of apparent reaction orders for water should account for different reaction mechanisms as a function of the support.

However our data do not support the assumption of Phatak et al. [42] on different reaction mechanisms as a function of support nature since the same catalyst a 2%$Pt/CeO_2/Al_2O_3$ catalyst, placed or not on top of the Ce/Al buffer layer, is used for all the experiments. On submitting this catalyst to the so-called "model" mixture conditions the presence of the buffer layer does not alter the catalytic activity and the reaction rate can be simulated using the rate law described in Eq. (3). However, in the presence of the surrogate feed stream the buffer layer alters the performances of the catalysts being now more active. A rate law similar to the previous one, Eq. (3), but increasing the reaction order for water, Eq. (5), can now fit the experimental data.

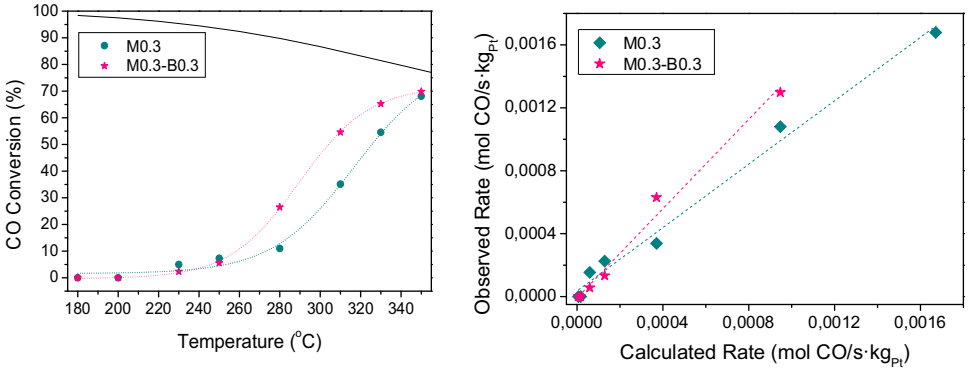

Fig. 10. (a) Effect of the buffer layer on the catalytic activity of M0.3 monolith, at WHSV = 80 L g^{-1} h^{-1} under a reactive flow of 50% H_2, 7% CO, 9% CO_2, 30% H_2O, balance N_2; (b) Observed vs. calculated CO conversions, assuming the rate law proposed by Germani et al. [40].

Table 3
Summary of reported reaction orders for Pt/Al_2O_3 and Pt/CeO_2 catalysts.

Catalyst	T (K)	Reaction order				E# (kJ mol^{-1})	Feed stream	Ref
		CO	H_2O	H_2	CO_2			
Pt/Al_2O_3	543	−0.21	0.75			84	24%CO 31%H_2O	[45]
1% Pt/Al_2O_3	558	0.06	1.00	−0.44	−0.10	68	7% CO 22% H_2O 8.5%	[46]
	588	0.10	1.10	−0.44	−0.07	84	CO_2 37% H_2	
1.66% Pt/Al_2O_3	558	0.11	0.82	−0.49	−0.06	81		
	573	0.10	0.77	−0.46	−0.08	81		
1% Pt/CeO_2	473	−0.03	0.44	−0.38	−0.09	75		
Pt/CeO_2	573	0	1			47	2.6%CO 2.0%H_2O	[52]
2%$Pt/Ce_{0.5}Zr_{0.5}O_2$	513–573	0.07	0.67	−0.57	−0.16	73	1.5–4.0%CO 31–44%H_2O	[53]
2%$Pt_{0.66}Re_{0.33}$/ $Ce_{0.5}Zr_{0.5}O_2$	513–573	−0.05	0.85	−0.32	−0.05	73	7–22%CO_{2c} 39–63%H_2	
1.7% $Pt/CeO_2/Al_2O_3$	533	0.13	0.49	−0.45	−0.12	86	7% CO 30% H_2O 9% CO_2 50% H_2	[43]
1% Pt/CeO_2	473	−0.03	0.44	−0.48	−0.09	77	7% CO 22% H_2O 8.5%	[48]
	573	0.14	0.66	−0.54	−0.08	93	CO_2 37%H_2	

$$-r_{CO}\left(\frac{molCO}{s\cdot kg_{cat}}\right) = \left(1.3\cdot 10^6\right)\times\left(e^{-\frac{86000}{RT}}\right) \times CO^{0.13}\times H_2O^{\mathbf{0.69}}\times H_2^{-0.45}\times CO_2^{-0.12} \times\left(1-\frac{H_2\times CO_2}{K_{eq}\times CO\times H_2O}\right) \quad (5)$$

The increase in the apparent reaction order of water, in the presence of the buffer layer, should account for an increase on the availability of water at the metal/support interface.

In a recent paper Clay et al. [48] model the intrinsic WGS kinetics over Pt by DFT and compare their results with experimental ones. These authors utilize four pathways for modeling the microkinetics of the WGS reaction: the carboxyl, the carboxyl-hydroxyl, the redox and the dual hydroxyl paths. The best fitting model is the one considering the carboxyl intermediate pathway and water dissociation the rate-limiting step. According to this model, changes on the rate-limiting step depending on the CO coverage are possible, in such a way that at high CO partial pressures the rate-limiting step shifts from water activation to carboxyl formation. These shifts on the rate-limiting steps account for the dependency of the reaction orders on the reaction conditions, which determines the surface coverage and surface partial pressures as a key factor. Consequently, increased H_2 surface presence (as for example in our "real" mixture) should results in a water splitting inhibition.

Olimpiou et al. [49] use SSITKA methodology for investigating the "H-path", the reaction pathway of the WGS reaction that results in the formation of H_2 from H_2O. These authors estimate the coverage of H-containing species for γ-Al_2O_3-supported Pt and Rh and state that labile hydroxyl groups and H species coming from dissociated water are involved in the reaction. However, just a small fraction of these species under WGS reaction conditions are energetically able to diffuse towards the metal particle for producing H_2 gas [50,51].

DFT studies on model Pt/CeO_2 (111) catalysts suggest that adsorption of molecular water on stoichiometric ceria terraces is favored over dissociatively adsorbed water by 0.2 eV. However, on partially reduced CeO_2(111) surfaces water dissociation takes place readily [52]. A significant enhancement of the water splitting process on partially reduced ceria has been already reported [38,54–57]. Recently, Anarifard et al. [53] found for Pt/CeO_2 catalysts that on the ceria surface H_2O dissociates at the oxygen vacancies transferring the H atom to neighboring oxygen surface atoms and only when complete surface coverage is attained water dissociation occurs at the metal-support interface. The role of the oxygen vacancies has also been associated to the higher capacity of the support to stabilize the fragments originated in the water dissociation process. Co-adsorption effects of CO and H_2O are important in the WGS reaction by lowering the adsorption energy of CO molecules and facilitating the carboxyl dissociation step. This may explain the observed enhancement of the WGS activity for Pt/ceria based catalysts [25,54].

Extrapolating this discussion to our structured catalyst design, CeO_2/Al_2O_3 buffer layer should provide an increased number of sites for the adsorption of water molecules. If an out-gas reformate feed stream is submitted to the WGS catalysts the high partial pressure of H_2 will results in the formation of partially reduced ceria surfaces favoring then water dissociation and stabilization on the support and on the buffer layer [50,53,58]. Moreover, the increased number of oxygen vacancies leads to an increase in the electronic densities of the metal particles [25,59–62]. The higher electron

density of the metal particles also hinder the H_2 absorption due to its donor character allowing a decrease on the surface coverage of hydrogen atoms and hence, an increased number of surface sites available for CO adsorption while simultaneously reducing the binding energy of CO on platinum. Similar conclusions were established by Liu et al. [45] indicating that increased electron densities on platinum active sites leads to higher selectivities on PrOx reaction by decreasing the H_2-metal interaction strength. However, this effect is independent on the presence of the buffer layer and, therefore, cannot explain by itself the enhanced activity due to the presence of this layer.

Assuming that the rate-limiting step is the transfer of hydroxyl groups to the metal-support interface and that surface diffusion rates are much higher than the reaction rates, an increased number of surface sites able of dissociating water molecules should provide and increased number of hydroxyl species at the metal particle periphery thus increasing the WGS reaction rate. The surface diffusion follows Fick's laws and therefore diffusion rate increase as the temperature increase.

4. Conclusions

The incorporation of the buffer layer to the system leads to different behavior as a function of the test conditions. In "model" mixture the best performance is obtained without buffer incorporated in the monolith. On the contrary, the buffer layer leads to an enhancement of the catalytic activity in "real" conditions. From the feed stream variations experiments, higher catalytic efficiency was observed for the bilayer micromonoliths in the presence of H_2 and CO_2.

The beneficial effects of the buffer layer are closely related to the presence of an extra number of cerium oxide defects and their associated electronic properties, which results in changes on the catalytic coverages. These changes could, indeed, increase the positive reaction order generally identified for H_2O species making that the resulted water partial pressures higher on the catalytic active sites. Hence, the main contribution of the buffer layer is associated to its capacity for dissociating water under reductive atmospheres. Higher number of oxygen vacancies allows higher water species surface diffusion rate to the metal-support interface thus increasing the WGS reaction rate.

In conclusion, structured catalytic system able to increase the activity in H_2-rich feed streams was successfully achieved. Although further studies are required, the bilayered micromonolithic catalysts, as a novel approach, become an interesting catalytic strategy on the real WGS process intensification.

Acknowledgement

The authors acknowledge Junta de Andalucía for the financial support (TEP-8196 project and TEP 106 group).

References

[1] R.J. Farrauto, Y. Liu, W. Ruettinger, O. Ilinich, L. Shore, T. Giroux, Catal. Rev. 49 (2007) 141–196.
[2] D.H. Prasad, J. Lee, H. Lee, B. Kim, J. Park, J. Ceram. Process. Res. 10 (2009) 748.
[3] J.V.G. Lietz, H. Lieske, H. Spindler, W. Hanke, J. Völter, J. Catal. 81 (1983) 17.
[4] S. Ivanova, O.H. Laguna, M.Á. Centeno, A. Eleta, M. Montes, J.A. Odriozola, Renewable Hydrogen Technologies, in: G. Gandía, P.M. Arzamendi (Eds.), Elsevier B.V., 2003, pp. 225–244.
[5] Q. Fu, H. Saltsburg, M. Flytzani-Stephanopoulos, Science 301 (2003) 935.
[6] A.Y. Tonkovich, J.L. Zilka, M.J. LaMont, Y. Wang, R.S. Wegeng, Chem. Eng. Sci. 54 (1999) 2947.
[7] W. Ruettinger, X. Liu, X. Xu, R.J. Farrauto, Topics Catal. 51 (2008) 60.
[8] A. Cybulski, J.A. Moulijn, Chem. Eng. Sci. 49 (1994) 19.
[9] E. Tronconi, G. Groppi, Chem. Eng. Sci. 55 (2000) 6021.
[10] H.J. Grabke, Mater. Corros. 49 (1998) 303–308.
[11] S. Strauss, R. Krajak, M. Palm, H.J. Grabke, Mater. Corros. 47 (1996) 701–702.
[12] D. Ugues, S. Specchia, G. Saracco, Ind. Eng. Chem. Res. 43 (2004) 1990–1998.
[13] M.I. Domiínguez, A. Peírez, M.A. Centeno, J.A. Odriozola, Appl. Catal. A: Gen. 78 (2014) 45–57.
[14] C. Ratnasamy, J.P. Wagner, Catal. Rev. 51 (2009) 325.
[15] A.S. Quiney, G. Germani, Y. Schuurman, J. Power Sour. 160 (2006) 1163.
[16] L.M. Martínez Tejada, M.I. Domínguez, O. Sanz, M.A. Centeno, J.A. Odriozola, Gold Bull. 46 (2013) 221.
[17] O.H. Laguna, M. González Castaño, M.A. Centeno, J.A. Odriozola, Chem. Eng. J. 275 (2015) 45.
[18] A.A. Gokhale, J.A. Dumesic, M. Mavrikakis, J. Am. Chem. Soc. 130 (2008) 1402.
[19] R.J. Madon, D. Braden, S. Kandoi, P. Nagel, M. Mavrikakis, J.A. Dumesic, J. Catal. 281 (2011) 1.
[20] C.H. Lin, C.L. Chen, J.H. Wang, J. Phys. Chem. C 115 (2011) 18582.
[21] S.C. Huang, C.H. Lin, J.H. Wang, J. Phys. Chem. C 114 (2010) 9826.
[22] A. Phatak, W. Delgass, J. Phys. Chem. C 113 (2009) 7269.
[23] X. Wang, R.J. Gorte, J.P. Wagner, J. Catal. 212 (2002) 225.
[24] J.A. Rodriguez, S. Ma, P. Liu, J. Hrbek, J. Evans, M. Pérez, Science 318 (2007) 1757.
[25] M. Gonzalez Castaño, T.R. Reina, S. Ivanova, M.A. Centeno, J.A. Odriozola, J. Catal. 314 (2014) 1.
[26] I. Barrio, I. Legorburu, M. Montes, M.I. Dominguez, M.A. Centeno, J.A. Odriozola, Catal. Lett. 101 (2005) 151.
[27] L.M. Martinez T, D.M. Frias, M.A. Centeno, A. Paul, M. Montes, J.A. Odriozola, Chem. Eng. J. 136 (2008) 390.
[28] V.G. Milt, S. Ivanova, O. Sanz, M.I. Domínguez, A. Corrales, J.A. Odriozola, M.A. Centeno, Appl. Surf. Sci. 270 (2013) 169.
[29] L.M. Martínez T, O. Sanz, M.I. Domínguez, M.A. Centeno, J.A. Odriozola, Chem. Eng. J. 148 (2009) 191–200.
[30] O. Sanz, F.J. Echave, F. Romero-Sarria, J.A. Odriozola, M. Montes, Renewable, in: L.M. Gandía, G. Arzamendi, P.M. Dieguez (Eds.), Hydrogen Technologies, Elsevier B.V., 2013, 2016, pp. 201–224.
[31] P.L. Mills, J.F. Nicole, Ind. Eng. Chem. Res. 44 (2005) 6453–6465.
[32] D.M. Frıas, S. Nousir, I. Barrio, M. Montes, L.M. Martınez, M.A. Centeno, J.A. Odriozola, Appl. Catal. A Gen. 325 (2007) 205–212.
[33] L.M. Martınez, O. Sanz, M.A. Centeno, J.A. Odriozola, Chem. Eng. J. 162 (2010) 1082–1090.
[34] M.I. Domínguez, A. Pérez, M.A. Centeno, J.A. Odriozola, Appl. Catal. B 478 (2014) 45.
[35] P.B. Weisz, J.S. Hicks, Chem. Eng. J. 17 (1961) 265.
[36] D.I. Potemkin, P.V. Snytnikov, V.D. Belyaev, V.A. Sobyanin, Chem. Eng. J. 176–177 (2011) 165.
[37] N. Dupont, G. Germani, A.C. van Veen, Y. Schuurman, G. Schäfer, C. Mirodatos, Int. J. Hydrogen Energy 32 (2007) 1443.
[38] C.M. Kalamaras, K.C. Petallidou, A.M. Efstathiou, Appl. Catal. B Environ. 136–137 (2013) 225.
[39] G. Jacobs, P.M. Patterson, U.M. Graham, D.E. Sparks, B.H. Davis, Appl. Catal. A Gen. 269 (2004) 63.
[40] G. Germani, P. Alphonse, M. Courty, Y. Schuurman, C. Mirodatos, Catal. Today 110 (2005) 114.
[41] D.C. Grenoble, M.M. Estadt, D.F. Ollis, J. Catal. 67 (1981) 90.
[42] A.A. Phatak, N. Koryabkina, S. Rai, J.L. Ratts, W. Ruettinger, R.J. Farrauto, G.E. Blau, W.N. Delgass, F.H. Ribeiro, Catal. Today 123 (2007) 224.
[43] X. Zheng, J. Mantzaras, R. Bombach, Combust. Flame 161 (2014) 332.
[44] S. Aranifard, S.C. Ammal, A. Heyden, J. Phys. Chem. C 116 (2012) 9029.
[45] X. Liu, O. Korotkikh, R. Farrauto, Appl. Catal. A Gen. 226 (2002) 293.
[46] L. Grabow, Y. Xu, M. Mavrikakis, Phys. Chem. Chem. Phys. 8 (2006) 3369.
[47] P. Thormählen, M. Skoglundh, E. Fridell, B. Andersson, J. Catal. 188 (1999) 300.
[48] J.P. Clay, J.P. Greeley, F.H. Ribeiro, W.N. Delgass, W.F. Schneider, J. Catal. 320 (2014) 106.
[49] G.G. Olympiou, C.M. Kalamaras, C.D. Zeinalipour-Yazdi, A.M. Efstathiou, Catal. Today 127 (2007) 304.
[50] D. Martin, D. Duprez, J. Phys. Chem. B 112 (2006) 4428.
[51] D. Duprez, Catal. Today 112 (2006) 17.
[52] Y. Lykhach, V. Johánek, H.A. Aleksandrov, S.M. Kozlov, M. Happel, T. Skála, P. St Petkov, N. Tsud, G.N. Vayssilov, K.C. Prince, K.M. Neyman, V. Matolín, J. Libuda, J. Phys. Chem. C 116 (2012) 12103.
[53] S. Aranifard, S.C. Ammal, A. Heyden, J. Phys. Chem. C 118 (2014) 6314.
[54] G. Jacobs, U.M. Graham, E. Chenu, P.M. Patterson, A. Dozier, B.H. Davis, J. Catal. 229 (2005) 499.
[55] T.R. Reina, W. Xu, S. Ivanova, M.Á. Centeno, J. Hanson, J.A. Rodriguez, J.A. Odriozola, Catal. Today 205 (2013) 41.
[56] A. Trovarelli, Catal. Rev. 38 (2006) 439.
[57] J.A. Rodriguez, J.C. Hanson, D. Stacchiola, S.D. Senanayake, Phys. Chem. Chem. Phys. 15 (2013) 12004.
[58] G. Jacobs, P.M. Patterson, L. Williams, E. Chenu, D. Sparks, G. Thomas, B.H. Davis, Appl. Catal. A Gen. 262 (2004) 177.
[59] S.M. Opalka, T.H. Vanderspurt, R. Radhakrishnan, Y. She, R.R. Willigan, J. Phys. Condens. Matter 20 (2008) 064237.
[60] F.W. Poulsen, M. Glerup, P. Holtappels, Solid State Ionics 135 (2000) 595.
[61] C.T. Campbell, C.H.F. Peden, Science 309 (2005) 713.
[62] Z.V. Popović, Z.D. Dohčević-Mitrović, N. Paunović, M. Radović, Phys. Rev. B Condens. Matter Mater. Phys. 85 (2012) 1.